Seismic resilience of concrete structures under corrosion

Fabio Biondini, Elena Camnasio and Andrea Titi*,†

Department of Civil and Environmental Engineering, Politecnico di Milano, Milan, 20133, Italy

Received 1 August 2014; Revised 6 May 2015; Accepted 10 May 2015

1. INTRODUCTION

The detrimental effects of aging and deterioration processes due to aggressive chemical attacks and other physical damage mechanisms can lead structure and infrastructure systems to exhibit over time unsatisfactory performance under service loadings or accidental actions and extreme events, such as earthquakes [1, 2]. During the last decades, risk assessment and mitigation programs have been carried out in the attempt to reduce future losses and post-disaster recovery costs [3–6]. In this context, the concept of resilience gained increasing importance in design, assessment, maintenance, and rehabilitation of structure and infrastructure systems. Resilience is a broad multidimensional concept that was introduced by Holling [7] in 1973 to ecology and has evolved from the disciplines of materials science and environmental studies to become extensively used and applied to several engineering branches [8, 9]. In the field of disaster mitigation, frameworks have been proposed to provide a basis for development of qualitative and quantitative models measuring the functionality and resilience at various scales, including components, groups, and systems within infrastructure networks and communities [10–15]. For the purpose of the discussion presented in this paper, resilience can be regarded as the capability of structures, infrastructure systems, and entire communities, to withstand the effects of extreme events and to recover efficiently the original performance and functionality [10, 14, 16, 17].

Resilience of critical facilities, such as hospitals and infrastructure networks, is often investigated with reference to damage and disruption caused by seismic events [10, 14, 16–22]. However, the effects of aging and environmental aggressiveness, which can modify the seismic performance and

*Correspondence to: Andrea Titi, Department of Civil and Environmental Engineering, Politecnico di Milano, Piazza Leonardo da Vinci 32, Milan, 20133, Italy.

†E-mail: andrea.titi@polimi.it

functionality and, consequently, make the system resilience depending on the time of occurrence of the seismic event, are not explicitly considered. In particular, for concrete structures, the exposure to the diffusive attack from aggressive agents, such as chlorides, may involve corrosion of steel reinforcement and deterioration of concrete that reduce over time the structural resources and affect the system resilience [23]. Therefore, a proper quantification of the seismic resilience of deteriorating structures must be based on the assessment of the structural system over its entire life-cycle by taking into account the effects of deterioration processes, time-variant loadings, and maintenance and repair interventions under uncertainty. To meet this need, a probabilistic approach to lifetime assessment of seismic resilience of concrete structures considering the interaction of environmental and seismic hazards is presented in this paper. This approach is based on a general methodology for life-cycle analysis of concrete structures exposed to aggressive environments [24–28]. The time-variant seismic capacity associated with different limit states, from damage limitation up to collapse, is assumed as functionality indicator, and the seismic resilience of the deteriorating system is computed over the structural lifetime with respect to this indicator by relating the post-event residual functionality and the recovery process to the time of occurrence of the seismic event.

The proposed approach is applied to probabilistic assessment of seismic resilience of a three-story concrete frame building and a four-span continuous concrete bridge under chloride-induced corrosion over a 50-year lifetime. The random variability in the material and geometrical properties and in the physical quantities of the deterioration process is considered. Parametric analyses based on Monte Carlo simulation are carried out to investigate the effects of the functionality loss, the recovery profile, and the post-recovery functionality target on the time-variant seismic resilience. The lifetime resilience under environmental and seismic hazards is then evaluated by taking the combined effects of structural deterioration and seismic damage into account based on a sequence of nonlinear dynamic analysis and post-event nonlinear static analysis. The results show that the seismic damage and the residual seismic capacity vary over time depending on structural deterioration. As a consequence, structures designed for the same functionality target could exhibit over time different functionality and seismic resilience depending on the environmental exposure. This indicates the importance of a multi-hazard life-cycle-oriented approach to seismic design of resilient structure and infrastructure systems.

2. RESILIENCE OF DETERIORATING STRUCTURES

2.1. Definition and measure of resilience

Let $Q = Q(t)$ be a time-variant functionality indicator in the range [0;1], with $Q = 1$ for undamaged systems and $Q = 0$ for fully damaged systems. The occurrence of an extreme event at time t_0 may cause a sudden loss ΔQ of system functionality. As shown in Figure 1, the loss ΔQ can be totally or partially recovered by post-event restoration activities over a recovery time interval $\delta_r = t_f - t_i$, where

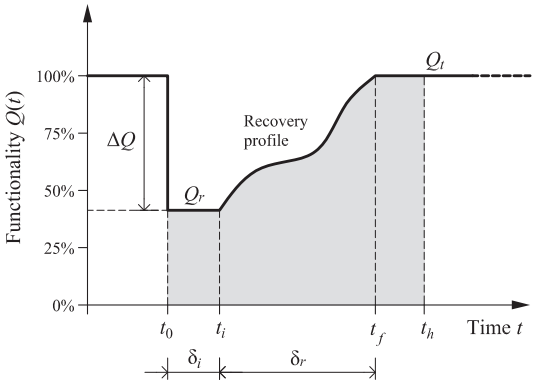

Figure 1. System functionality and definition of resilience.

$t_i = t_0 + \delta_i$ and t_f are the initial and final time of the restoration process, respectively, and δ_i is the idle time or the elapsed time between the occurrence of the extreme event and the beginning of the recovery process.

Resilience can be defined as the capability of the system to sustain the effects ΔQ of the extreme event at time t_0 and to recover efficiently a target level of functionality Q_t at time t_f. Based on this definition, an effective dimensionless measure of resilience is given by an average value of the post-event functionality $Q = Q(t)$ over a time horizon $t_h \geq t_f$ [16, 17]:

$$R = \frac{1}{t_h - t_0} \int_{t_0}^{t_h} Q(t) dt. \tag{1}$$

This concept is shown in Figure 1, where resilience is associated with the area underlying the functionality profile over the time interval $[t_0; t_h]$. The practical applicability of this qualitative and quantitative definition of resilience has been shown in literature for existing structures and real infrastructure networks [14, 17, 21, 22].

2.2. *Time-variant resilience*

Resilience should measure the ability of a system exposed to hazards to resist extreme events and recover its functionality in a timely and efficient manner [29]. Therefore, for structures in aggressive environment, the quantification of resilience should account also for the environmental hazard. Despite this evidence, resilience is generally investigated by assuming a time-invariant functionality before the occurrence of an extreme event and after the completion of the restoration process. According to this assumption, resilience depends on the recovery profile $Q = Q(t)$ over the time interval $[t_0, t_h]$, and it is independent on the time t_0 of occurrence of the extreme event (Figure 2(a)). However, the effects of damage due to environmental aggressiveness could reduce over time the system functionality and, consequently, modify the functionality loss induced by extreme events of same magnitude (Figure 2(b)). Therefore, the pre-event functionality of deteriorating structures is time-variant, and resilience is depending on the time of occurrence t_0 [23, 30].

The time-variant resilience $R = R(t_0)$ depends on several factors related to both the deterioration process and the effectiveness of the recovery process. In general, the structural system suffers an increasing decay of performance in terms of both functionality and resilience as the severity of the environmental exposure increases (Figure 3(a)). If the functionality indicator falls below an acceptable target threshold before an extreme event occurs, maintenance or repair interventions should be carried out to restore suitable levels of system functionality Q_m and to improve resilience (Figure 3(b)). Preventive and/or essential maintenance programs, usually applied to preserve the structural safety and serviceability and extending the structural lifetime of deteriorating structures, can be planned to this purpose based on established maintenance models [31, 32]. The applications presented in this paper will focus on lifetime assessment of resilience under no maintenance, that is particularly relevant for the condition rating of existing structures and infrastructure systems,

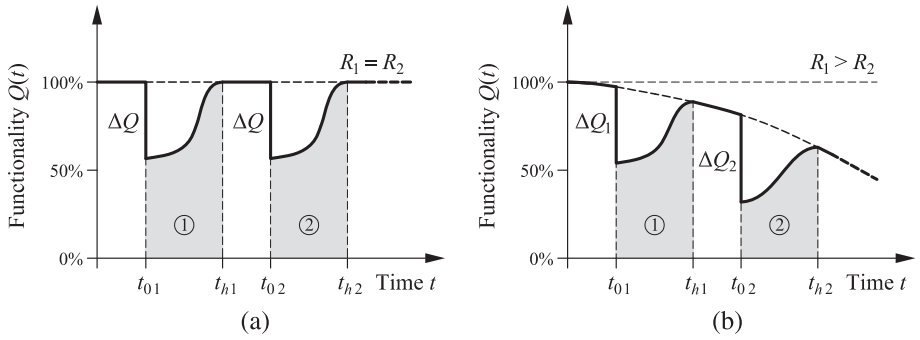

Figure 2. Functionality Q and functionality losses ΔQ_k due to the occurrence of extreme events $k = 1,2,\ldots$, of same magnitude at different time instants $t_{0,k}$ and recovery over the time intervals $[t_{i,k}; t_{f,k}]$, with $t_{i,k} = t_{0,k}$ and $t_{f,k} = t_{h,k}$. (a) Non-deteriorating system and (b) deteriorating system.

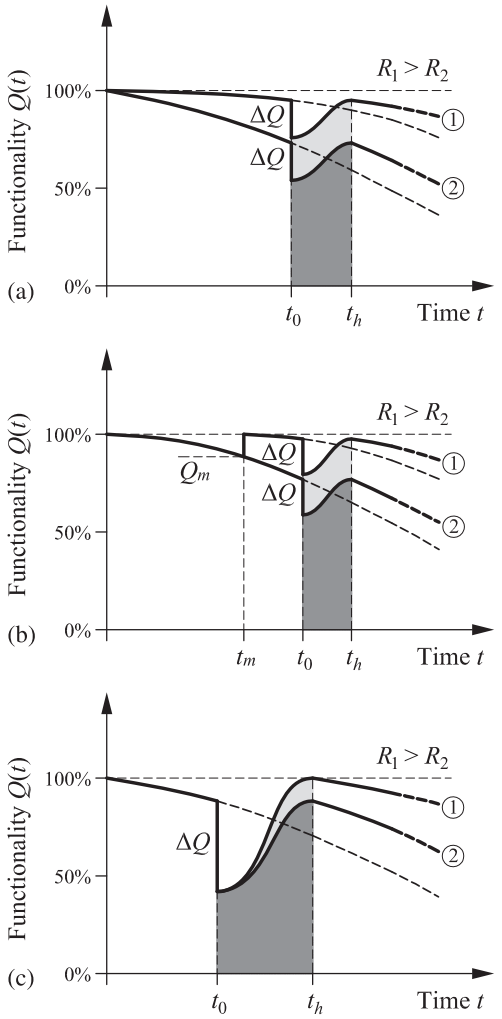

Figure 3. Effects of the deterioration process and related factors on the time-variant system functionality $Q = Q(t)$ and resilience $R = R(t_0)$. (a) Environmental aggressiveness with ① slight/moderate exposure or ② severe exposure. (b) Maintenance programs ① with and ② without repair interventions. (c) Post-event recovery actions with ① total restoring of the initial functionality or ② partial restoring of the pre-event functionality.

including buildings, bridges, roads, railways, dams, ports, and other critical facilities [33]. However, it is clear that maintenance models can be easily incorporated in the proposed approach based on a proper updating of the time-variant system performance and functionality profiles.

The functionality level Q_t targeted by post-event interventions is also an important decisional parameter that affects the time evolution of resilience. It is worth noting that the target functionality should be chosen based not only on available resources, time limitations, and importance of the structure but also on the impact of structural deterioration. As an example, post-recovery actions may involve a total restoring of the initial functionality of the undamaged system or a partial recovery up to the pre-event functionality of the damaged system (Figure 3(c)).

3. FRAMEWORK FOR SEISMIC RESILIENCE ASSESSMENT

3.1. Functionality indicators

In literature, several functionality indicators have been used for resilience assessment [18, 19, 22, 34–39]. For deteriorating structures in seismic areas, it is appropriate to relate the time-variant system functionality

$Q = Q(t)$ to the residual seismic capacity in terms of peak ground acceleration $a_g = a_g(t)$ associated with the reaching of prescribed limit states, from damage limitation up to collapse. Different limit states could be established for buildings, bridges, and other structures depending on the structural typology [40]. Table I provides an example of structural performance levels and limit states identified with respect to the displacement demand, where Δ_y and Δ_u are the displacement capacities of the structural system at first yielding and ultimate states, respectively, and $\Delta_p = \Delta_u - \Delta_y$ is the available plastic displacement [28].

Due to aging and deterioration processes, the seismic capacity $a_g = a_g(t)$ decreases over time from the initial value $a_{g,0} = a_g(0)$ of the undamaged system down to capacity levels that may involve a loss of system functionality $Q = Q(t)$. The decrease of functionality in the range [0;1] can be related to the residual seismic capacity over a suitable interval of limit values $[a_{g,\min}; a_{g,\max}]$, as qualitatively shown in Figures 4(a) and 4(b).

Depending on the type of structure, a continuous nonlinear or constant stepwise relationship $Q = Q(a_g)$ could be chosen based on the definition of a suitable set of seismic capacity thresholds and discrete functionality states, as qualitatively shown in Figure 5(a) for a five-level damage state thresholding. In practice, this approach is useful in post-earthquake evaluation procedures with damage levels qualitatively assessed by visual inspection. Table II gives an example of observed damage states and related repair interventions for bridge systems [40], with estimation of the bridge outage [41].

However, when a direct assessment of the seismic capacity is feasible, a linear relationship could be effectively adopted for resilience assessment, as shown in Figure 5(b). In addition, in most cases, full functionality is associated with the availability of the initial seismic capacity or $a_{g,\max} = a_{g,0}$, and complete loss of functionality occurs at structural collapse or $a_{g,\min} = 0$. Therefore, for the purpose of the present study, the following linear relationship is assumed [23]:

$$Q(t) = \frac{a_g(t)}{a_{g,0}}. \tag{2}$$

3.2. Time-variant seismic capacity and functionality losses

The time-variant seismic capacity $a_g = a_g(t)$ under prescribed ground motions can be evaluated through incremental nonlinear dynamic analysis of the deteriorating system by increasing the peak ground acceleration up to the reaching of the investigated limit state. Nonlinear static analysis can also

Table I. Limit states and corresponding system displacement limits.

Performance level	Limit state	Displacement limit
SP-1	Fully operational	Δ_y
SP-2	Operational	$\Delta_y + 0.3\Delta_p$
SP-3	Life safe	$\Delta_y + 0.6\Delta_p$
SP-4	Near collapse	$\Delta_y + 0.8\Delta_p$
SP-5	Collapse	$\Delta_u = \Delta_y + \Delta_p$

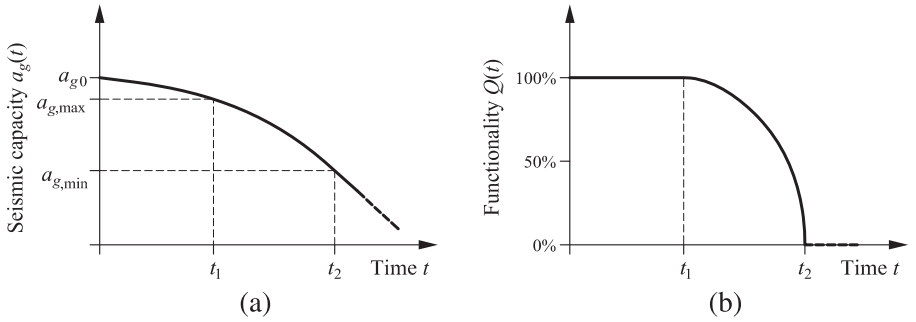

Figure 4. Time evolution of (a) seismic capacity $a_g = a_g(t)$ and (b) corresponding system functionality $Q = Q(t)$ for deteriorating structures.

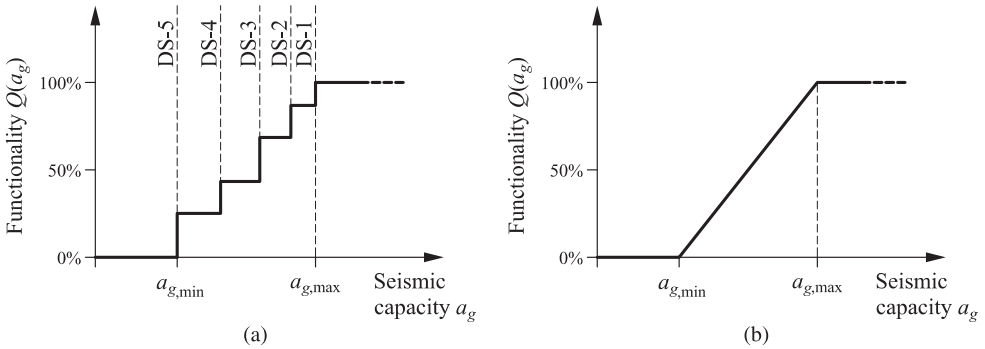

Figure 5. (a) Constant stepwise and (b) linear relationship of system functionality $Q=Q(t)$ versus residual seismic capacity $a_g=a_g(t)$.

Table II. Damage states, type of failures, repair interventions, and outage for bridges. Adapted from [40, 41].

Damage state	Failure mechanism	Repair required	Outage
DS-1	Pre-yielding	None	*None*
DS-2	Minor spalling	Inspect, patch	*<3 days*
DS-3	Bar buckling	Repair components	*<3 weeks*
DS-4	Bar fracture	Rebuild components	*<3 months*
DS-5	Collapse	Rebuild structure	*>3 months*

provide information on the time-variant base shear ultimate capacity $F_u=F_u(t)$ of the deteriorating structural system provided that certain prerequisites on the system ductility are satisfied. In fact, for the collapse limit state, the seismic capacity a_g can be conveniently related to the base shear capacity F_u by means of the design response spectrum as follows [42]:

$$F_u = \frac{\beta(T_1)}{q(\mu_\Delta)} m a_g, \tag{3}$$

where $\beta=\beta(T_1)$ is the elastic response spectrum function depending on the first vibration period T_1 of the structure, $q=q(\mu_\Delta)$ is the behavior factor depending on the displacement ductility μ_Δ of the earthquake-resisting system, and m is the seismic mass. For the evaluation of the behavior factor, the displacement ductility $\mu_\Delta=\Delta_u^*/\Delta_y^*$ refers to an equivalent elastic-plastic model of the base shear force versus displacement capacity curve. The yielding displacement Δ_y^* is estimated on a bilinear model with equal strength and equal dissipated energy up to the displacement at the peak force of the actual capacity curve, as proposed in [43]. The ultimate displacement Δ_u^* is associated with the point of the capacity curve where the total base shear force drops to 80% of the peak value.

For relatively flexible structures with high vibration periods, as those considered in this study, the equal displacement principle with $q=\mu_\Delta$ can be assumed [44]. Moreover, for concrete structures exposed to corrosion, it is expected that deterioration does not affect significantly the vibration period T_1. Under these assumptions, the time-variant functionality indicator can be formulated as follows:

$$Q(t) = \frac{a_g(t)}{a_{g,0}} = \frac{F_u(t)\mu_\Delta(t)}{F_{u,0}\mu_{\Delta,0}}, \tag{4}$$

where $F_u=F_u(t)$ and $\mu_\Delta=\mu_\Delta(t)$ are the time-variant base shear capacity and displacement ductility of the deteriorating structural system, respectively, with $F_{u,0}=F(0)$ and $\mu_{\Delta,0}=\mu_\Delta(0)$.

Nonlinear dynamic time-history analysis provides comprehensive information about the structural performance under ground motion, including a direct measure of the seismic damage, but it is computationally expensive. Nonlinear static analysis generally involves a lower computational cost and could be more conveniently used within a probabilistic framework for resilience assessment. However, it does not allow a direct estimation of seismic damage. Therefore, to benefit from the

advantages of both approaches, the residual functionality $Q_r = Q_r(t_0)$ after occurrence of a seismic event at time t_0 could be evaluated by performing in sequence a nonlinear dynamic time-history analysis, to assess the seismic damage, and a nonlinear static analysis, to evaluate the post-event residual seismic capacity [23]. This procedure can also be used to account for the cumulative seismic damage consequent to mainshock–aftershock sequences.

3.3. Recovery functions

After an extreme event, different functionality recovery profiles can be adopted depending on the magnitude, type and location of damage, and restoring procedures [16, 17]. In particular, the rapidity of the recovery process is related to several factors [19], such as the resources available after the event, the functionality of the infrastructure network, the importance of the structure, and the role of the damaged components in the system performance. In general, a functionality recovery model can be effectively represented as follows:

$$Q(\tau) = Q_r + H(\tau) r(\tau)\ (Q_t - Q_r), \tag{5}$$

where Q_r is the residual functionality at the initial time $t = t_i$ of the recovery process, Q_t is the target functionality at the end of the recovery time interval $\delta_r = t_f - t_i$, $\tau = (t - t_i)/\delta_r \in [0,1]$ is a normalized time variable, $H = H(\tau)$ is the Heaviside unit step function, and $r = r(\tau) \in [0;1]$ is a recovery function.

Effective functionality recovery models have been proposed in [16, 21], and [45]. In this paper, the role of the recovery process on the lifetime seismic resilience is investigated by considering the following recovery functions:

$$r(\tau) = 1 - e^{-k\tau} \quad \text{negative} - \text{exponential}, \tag{6}$$

$$r(\tau) = \frac{1 - \cos(\pi\tau)}{2} \quad \text{sinusoidal}, \tag{7}$$

$$r(\tau) = e^{-k(1-\tau)} \quad \text{positive} - \text{exponential}, \tag{8}$$

where k is a shape parameter. The type of the recovery actions should be selected according to the emergency response and recovery scenario based on the importance of the structure and the limit state to be restored. A proper tuning of the shape parameter k allows to effectively reproduce the planned recovery profile depending on magnitude and speed of the applied recovery actions. As an example, Figure 6 shows the three recovery models for $k = 10$. The negative-exponential-type function allows to reproduce recovery processes where most of functionality is restored quickly after the seismic event. The sinusoidal-type function describes a recovery process where functionality is restored gradually in time. Finally, the positive-exponential-type function well represents recovery processes where functionality is restored mainly at the end of the recovery time interval.

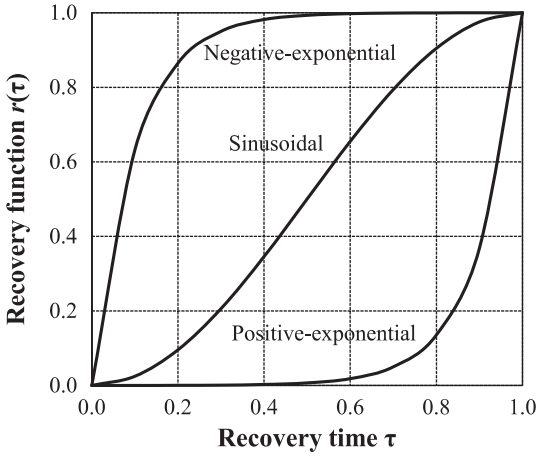

Figure 6. Functionality recovery profiles ($k = 10$).

4. DETERIORATION MODELING IN CONCRETE STRUCTURES UNDER DIFFUSION-CONTROLLED CORROSION

Chloride-induced corrosion represents a critical issue for huge stocks of existing concrete structures [33]. The local damage at the material level or member level is reflected at the global level leading to time-variant structural performance under service loadings, accidental actions, and extreme events, such as earthquakes. The detrimental effects of corrosion processes on the energy dissipation capacity of the earthquake-resisting system can seriously affect the seismic capacity of frame buildings and bridges [27, 28, 46–48]. In this paper, the time-variant seismic performance is evaluated at the system level based on a general approach to lifetime assessment of concrete structures in aggressive environment [24–26, 28]. This approach accounts for both the diffusion process of the aggressive agent, such as chlorides, and the mechanical damage induced by diffusion, which involves corrosion of reinforcement and deterioration of concrete. The different sources of uncertainty related to random variability of material and geometrical properties, environmental exposure, diffusion process, and earthquake excitation are taken into account based on a probabilistic modeling of the involved random variables.

4.1. Diffusion process

The transport of chlorides in concrete is diffusion-controlled and can be modeled by Fick's laws [49]. For a single component diffusion in isotropic, homogeneous, and time-invariant media, Fick's model is described by the following second order partial differential linear equation [50]:

$$D\nabla^2 C = \frac{\partial C}{\partial t}, \tag{9}$$

where D is the diffusivity coefficient of the medium, $C = C(\mathbf{x},t)$ is the concentration of the chemical component at point $\mathbf{x}$ and time t, $\nabla C = \mathbf{grad}\ C(\mathbf{x},t)$ and $\nabla^2 = \nabla \cdot \nabla$. Such equation can effectively reproduce the two-dimensional or three-dimensional patterns of concentration gradients that generally occur in concrete structures [24, 25]. However, depending on the exposure scenario and the geometry of concrete members, a simplified one-dimensional Fick's model may provide suitable accuracy in the description of the diffusion process [51]. Fick's equation in one dimension is often applied for durability analysis of concrete structures because it can be integrated analytically to obtain the following limit state equation that provides the initiation time of chloride-induced corrosion [52]:

$$C(x = c, t) = C_0 + \left(C_{S,\Delta x} - C_0\right)\left[1 - \mathrm{erf}\ \frac{c - \Delta x}{2\sqrt{D_{app,C}\,t}}\right] = C_{crit}, \tag{10}$$

where erf(·) is the Gauss error function, $C(x = c, t)$ is the chloride concentration at the depth c of concrete cover and time t, C_{crit} is a critical threshold of chloride concentration, C_0 is the initial chloride content in the cement paste, Δx is the depth of the convection zone, that is the concrete layer up to which the process of chloride penetration differs from Fick's model, $C_{S,\Delta x}$ is the chloride content at depth Δx, and $D_{app,C}$ is the apparent chloride diffusion coefficient:

$$D_{app,C}(t) = D_{RCM}\left(\frac{t_{28}}{t}\right)^a, \tag{11}$$

where D_{RCM} is the rapid chloride migration coefficient, $t_{28} = 28\,\mathrm{days} = 0.0767\,\mathrm{years}$ is the reference initial time, and a is an aging coefficient. Further details can be found in [52].

4.2. Corrosion of reinforcing steel and deterioration of concrete

The main consequence of corrosion is the reduction of the cross-sectional area of the reinforcing steel bars [49]. Considering uniform corrosion, the time-variant diameter $\Phi = \Phi(t)$ of a corroded bar can be represented as a function of the corrosion penetration $P_x = P_x(t)$ as follows [28]:

$$\Phi(t) = \Phi_0 - 2P_x(t) = [1 - \delta(t)]\Phi_0, \tag{12}$$

where $\Phi_0 = \Phi(0)$ is the diameter of the undamaged steel bar and $\delta = \delta(t) \in [0;1]$ is a time-variant dimensionless corrosion penetration index:

$$\delta(t) = \frac{2P_x(t)}{\Phi_0}. \tag{13}$$

The variation over time of the cross-sectional area $A_s = A_s(t)$ of the corroded steel bar can also be described by means of a corrosion damage index $\delta_s = \delta_s(t) \in [0;1]$ as follows [24]:

$$A_s(t) = [1 - \delta_s(t)]A_{s,0}, \tag{14}$$

where $A_{s,0} = \pi\Phi_0^2/4$ is the area of the undamaged steel bar and

$$\delta_s(t) = [2 - \delta(t)]\delta(t). \tag{15}$$

The corrosion process causes also a reduction of steel ductility [53, 54]. Moreover, the formation of oxidation products may lead to propagation of longitudinal cracks and concrete cover spalling [55–57]. These effects are modeled based on experimental evidence through a reduction of the ultimate steel strain $\varepsilon_{su} = \varepsilon_{su}(t)$ and of the concrete strength $f_c = f_c(t)$ as a function of the cross-sectional damage index $\delta_s = \delta_s(t)$. The damage models $\varepsilon_{su} = \varepsilon_{su}(\delta_s)$ and $f_c = f_c(\delta_s)$ are described in [58].

Corrosion process starts once the chloride concentration $C = C(x,t)$ at the depth $x = c$ of the concrete cover reaches a critical value C_{crit} and evolves in time with a corrosion rate related to the time evolution of concentration. On the basis of available data on chloride attacks [49, 59–61], a linear relationship between the rate of corrosion in the range 0 to 200 μm/year and the chloride content, in the range of 0–3%, is approximately assumed in this study for structures exposed to severe environmental conditions [28].

Based on the proposed damage modeling, the effects of corrosion are implemented into structural analysis through damage indices at the material level. In this way, corrosion can selectively be applied to damaged structural members with a different level of penetration in each reinforcing steel bar and a different type of deterioration over the concrete volume, in order to consider prescribed damage patterns and corrosion levels [24]. The accuracy of this approach has been successfully validated with reference to experimental tests carried out on beams subjected to accelerated and natural corrosion [58]. In particular, the comparison of numerical and experimental results has demonstrated the accuracy and capability of the proposed models to reproduce the effects of local corrosion damage on the structural response at the system level. Further details about damage modeling for pitting corrosion and mixed types of uniform and pitting corrosion can also be found in [58].

5. APPLICATIONS

The seismic performance, functionality, and resilience of a concrete frame building and a concrete continuous bridge exposed to corrosion are investigated under different sources of uncertainty related to the random variability of material and geometrical properties, environmental exposure, diffusion process, and earthquake excitation.

5.1. Probabilistic modeling

The probabilistic model for material and geometrical properties assumes the following quantities as random variables: concrete compression strength f_c, steel yielding strength f_{sy}, coordinates (y_p, z_p) of the nodal points $p = 1,2,\ldots$ of the concrete cross section, and coordinates (y_m, z_m) and diameter Φ_m of the steel bars $m = 1,2,\ldots$. These variables are considered uncorrelated and modeled for the undamaged structure with the probabilistic distributions, mean, and standard deviation values listed in Table III [25].

The diffusion process is described in probabilistic terms as proposed in [52]. Severe exposure and spray conditions with $C_0 = 0$ and $\Delta x = 0$ are assumed. The following uncorrelated random variables are considered: concrete cover c, chloride migration coefficient D_{RCM}, aging coefficient a, chloride content $C_{s,\Delta x}$, and critical chloride content C_{crit}. The probabilistic distributions and their mean and standard deviation values are listed in Table IV [52]. The time-variant probabilistic assessment of

Table III. Probability distribution, mean μ, and standard deviation σ of material and geometrical properties [25].

Random variable	Distribution type	μ #	σ
Concrete strength, f_c [MPa]	Lognormal	$f_{c,nom}$	5
Steel strength, f_{sy} [MPa]	Lognormal	$f_{sy,nom}$	30
Coordinates of the nodal points, (y_p,z_p) [mm]	Normal	$(y_p,z_p)_{nom}$	5
Coordinates of the steel bars, (y_m,z_m) [mm]	Normal	$(y_m,z_m)_{nom}$	5
Steel bar diameter, Φ_m [mm]	Normal*	$\Phi_{m,nom}$	$0.10\,\mu$

*Truncated distribution with non-negative outcomes.
#*nom* = nominal value.

Table IV. Probability distribution, mean μ, and standard deviation σ of the parameters of the diffusion process and corrosion initiation [52].

Random variable	Distribution type	μ	σ
Concrete cover, c [mm]	Normal *	40	8
Chloride migration coefficient, D_{RCM} [m^2/s]	Normal *	15.8×10^{-12}	$0.20\,\mu$
Aging coefficient, a [-]	Beta [0.0; 1.0]#	0.3	0.12
Chloride content, $C_{s,\Delta x}$ [wt.%/cem]	Normal *	3	$0.30\,\mu$
Critical chloride content, C_{crit} [wt.%/cem]	Beta [0.2; 2.0]#	0.6	0.15

*Truncated distributions with non-negative outcomes.
#[Lower bound; Upper bound].

the seismic performance and of the associated system functionality and resilience is carried out based on the adopted probabilistic models by means of Monte Carlo simulation. The sample size of the simulation process is chosen to achieve convergence of the statistical parameters of the investigated quantities.

5.2. *Three-story concrete frame building*

The seismic resilience of the three-story concrete-frame building shown in Figure 7(a) is investigated over a 50-year lifetime. The seismic weights related to both dead and live loads lead to an axial compressive force $N = 250$ kN over the columns at each story level. The columns are considered to be exposed to a diffusive attack from chlorides on the outermost external sides only.

The columns have square cross-section 0.70×0.70 m and are reinforced with eight steel bars with nominal diameter $\Phi_{nom} = 22$ mm. The concrete core is confined by double layer stirrups Φ8/75 mm.

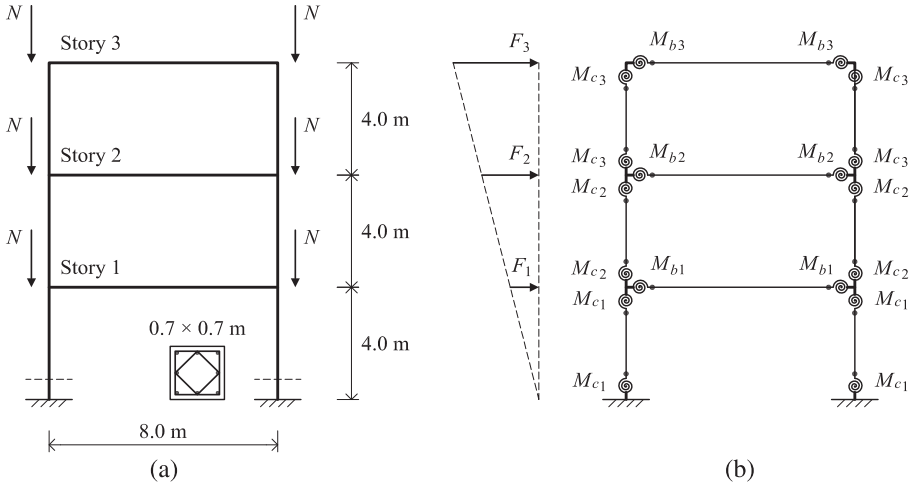

Figure 7. Three-story concrete-frame building. (a) Geometrical dimensions and column cross-section. (b) Structural modeling.

The nominal material strengths are $f_c = 35$ MPa and $f_{sy} = 435$ MPa. The limit state of failure of the cross-section is associated with the reaching of the strain limits of the materials. A basic value of ultimate strain $\varepsilon_{cu} = 0.35\%$ is assumed for concrete in compression. This limit is increased to account for the effects of confinement according to the model proposed in [62]. An ultimate strain $\varepsilon_{su} = 6.00\%$ is assumed for reinforcing steel of uncorroded bars.

The lifetime performance of the column cross-section is shown in Figure 8 in terms of nominal bending moment M_z versus curvature χ_z diagrams for $N = 500$ kN. The non-symmetric exposure leads over time to non-symmetric behavior. A significant reduction of bending strength, mainly due to the corrosion of the steel bars in tension and to the deterioration of concrete in compression, is observed for both positive and negative bending moments. In terms of curvature ductility, a significant deterioration is observed for negative bending moments only, because in this case failure is governed by the concrete crushing in the compressive zone close to the exposed side, with reduced confinement effects due to corrosion of the stirrups.

The beams have rectangular cross-section 0.50×0.80 m. Steel reinforcement is designed to achieve nominal bending strengths $M_{b1} = 1127.9$ kN, $M_{b2} = 985.6$ kN, and $M_{b3} = 457.1$ kN, with coefficient of variation of 15%. These values are selected to satisfy the 'strong columns-weak beams' capacity design criteria [44] with a 10% of over-strength. Based on these assumptions, the effects of the deterioration process at the system level are studied with reference to the structural model shown in Figure 7(b). Elastic beam elements with lumped inelastic rotational springs at member ends are used for both columns and beams to simulate the nonlinear behavior of the connections with formation of plastic hinges. The bending moment-rotation constitutive laws are described by a stepwise linearization of the bending moment-curvature relationships integrated over the length of the plastic hinge. Further details on the moment-rotation constitutive laws can be found in [30].

Nonlinear static analyses of the frame building under a triangular distribution of lateral story forces, as shown in Figure 7(b), are performed using the code Ruaumoko2D [63]. Figure 9 shows the lifetime performance of the building in terms of nominal base shear F_b versus top displacement Δ_t diagrams. It can be noticed a moderate decrease over time of the base shear capacity $F_u = F_u(t)$ and an abrupt reduction of the ultimate displacement, and hence of the displacement ductility $\mu_\Delta = \mu_\Delta(t)$, after about 20 years of lifetime. This is because of a change of the location of the flexural plastic hinges, which involves a consequent change of the collapse mechanism and energy dissipation capacity of the system. In fact, because of the reduction of the moment capacity of the columns, the system failure shifts from a 'beam-sway' to a 'column-sway' mechanism [27, 28]. This result clearly demonstrates that the seismic performance of concrete structures can be seriously affected by environmental hazards. It is worth noting that the reduction of shear strength of the columns, due to corrosion of the stirrups, can also modify the original capacity design and lead to brittle shear failures [42]. However, such circumstance can be excluded by comparing over time the shear strength of the columns at each story and the corresponding shear demand, as shown in [47].

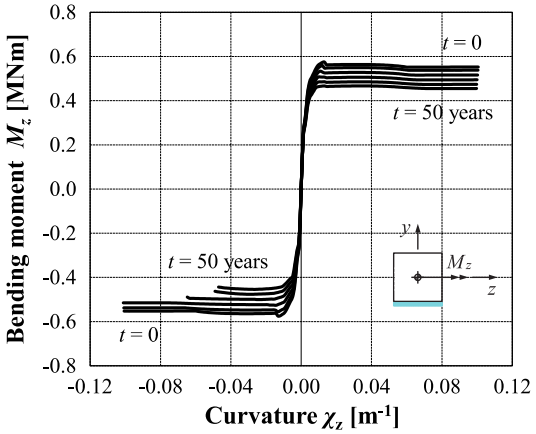

Figure 8. Column cross-section under corrosion. Nominal bending moment M_z versus curvature χ_z diagrams for $N = 500$ kN over a 50-year lifetime with time steps $\Delta t = 10$ years.

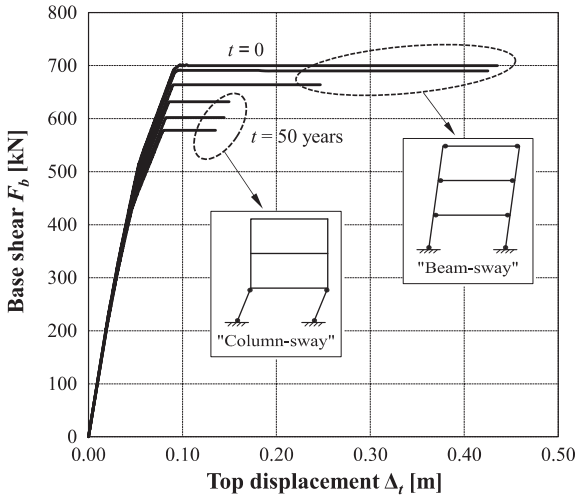

Figure 9. Frame building under corrosion. Nominal base shear F_b versus top displacement Δ_t over a 50-year lifetime with time steps $\Delta t = 10$ years.

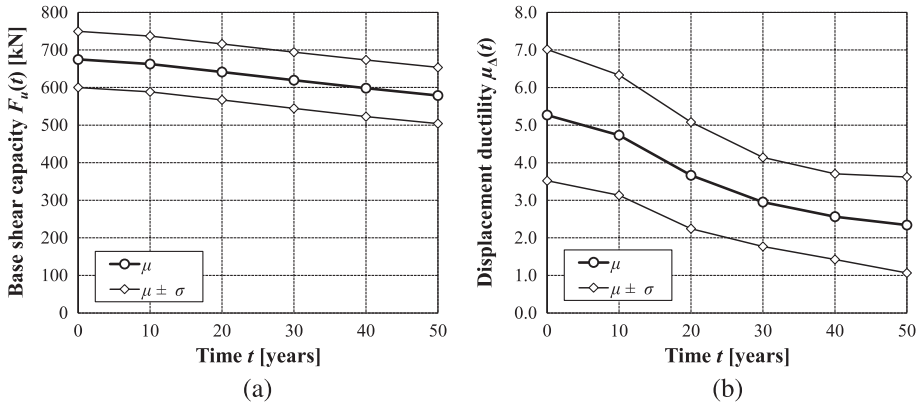

Figure 10. Frame building under corrosion. Time evolution of mean μ and standard deviation σ of (a) base shear capacity $F_u = F_u(t)$ and (b) displacement ductility $\mu_\Delta = \mu_\Delta(t)$.

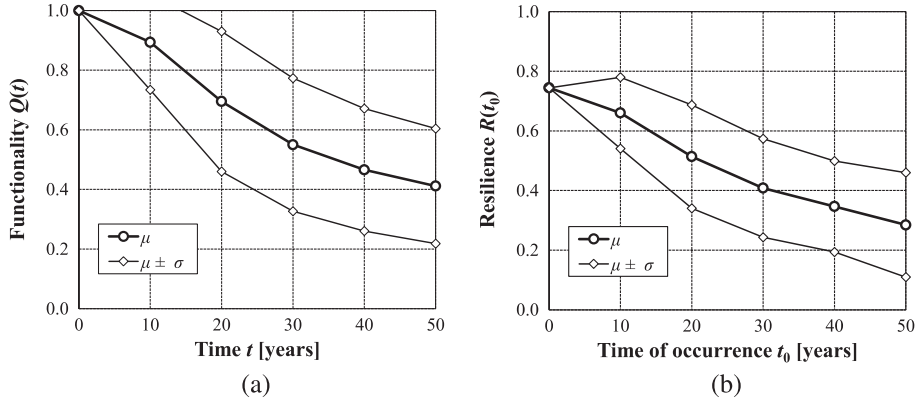

Figure 11. Frame building under corrosion. Time evolution of mean μ and standard deviation σ of (a) system functionality $Q = Q(t)$ and (b) seismic resilience $R = R(t_0)$ for the case of $t_i = t_0$, $t_h = t_f$, $\delta_r = 12$ months, functionality loss $\Delta Q(t_0) = 0.5 Q(t_0)$, and recovery process with sinusoidal profile and partial restoring aimed at recovering the pre-event functionality.

The same trends are confirmed also in probabilistic terms. Figure 10 shows the time evolution of the probabilistic parameters of the base shear capacity $F_u = F_u(t)$ and displacement ductility $\mu_\Delta = \mu_\Delta(t)$. The corresponding time evolution of the probabilistic parameters of the system functionality $Q = Q(t)$ associated with the performance functions $F_u = F_u(t)$ and $\mu_\Delta = \mu_\Delta(t)$ is shown in Figure 11(a). Over time, the mean value of the functionality decreases and the effects of uncertainty increase because of the deterioration process. Therefore, the probability distribution of seismic resilience $R = R(t_0)$ depends on the time t_0 of occurrence of the seismic event, as shown in Figure 11(b), for a case study with $t_i = t_0$, $t_h = t_f$, δ_r =12 months, functionality loss $\Delta Q(t_0) = 0.5Q(t_0)$, and recovery process with sinusoidal profile and partial restoring aimed at recovering the pre-event functionality. For a

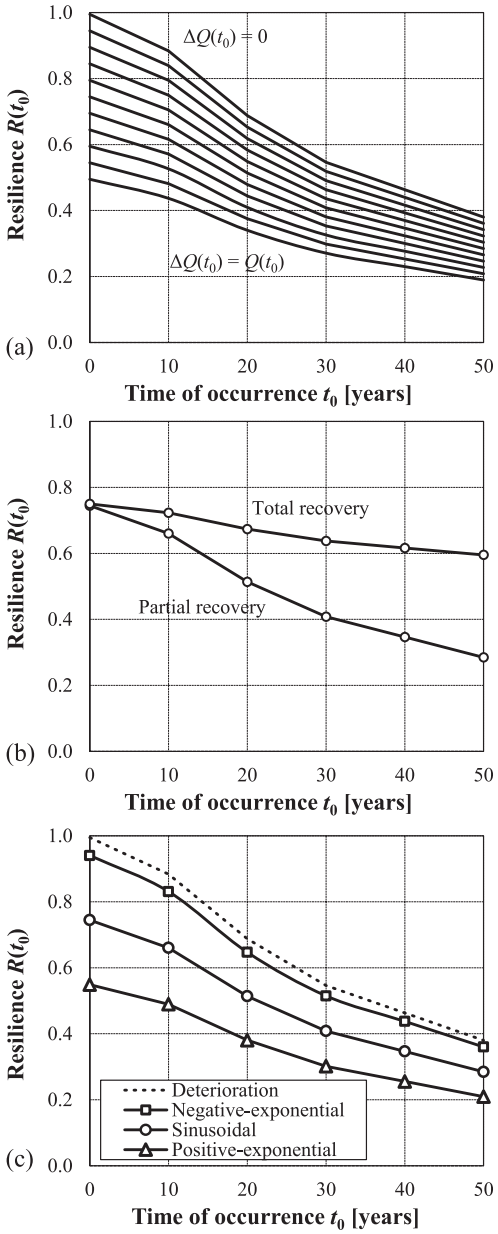

Figure 12. Frame building under corrosion. Time evolution of the mean value of seismic resilience $R = R(t_0)$ for $t_i = t_0$, $t_h = t_f$, and δ_r =12 months. (a) Functionality loss varying from $\Delta Q(t_0) = 0$ to $\Delta Q(t_0) = Q(t_0)$ with steps $0.1Q(t_0)$. (b) Target functionality with total restoring of the initial functionality $Q_t = 1.0$ and partial restoring of the pre-event functionality $Q_t = Q(t_0)$. (c) Recovery process $r = r(t)$ with negative-exponential, sinusoidal, and positive-exponential profiles ($k = 10$).

deterministic recovery process, the randomness of both system functionality and seismic resilience is due only to the uncertainty involved in the deterioration process. The effects of this kind of uncertainty lead over time to probability density distributions of functionality and resilience skewed toward the lower values of such indicators. In this regard, it is worth noting that the diagrams associated with the mean values plus one standard deviation shown in Figures 11(a) and 11(b)

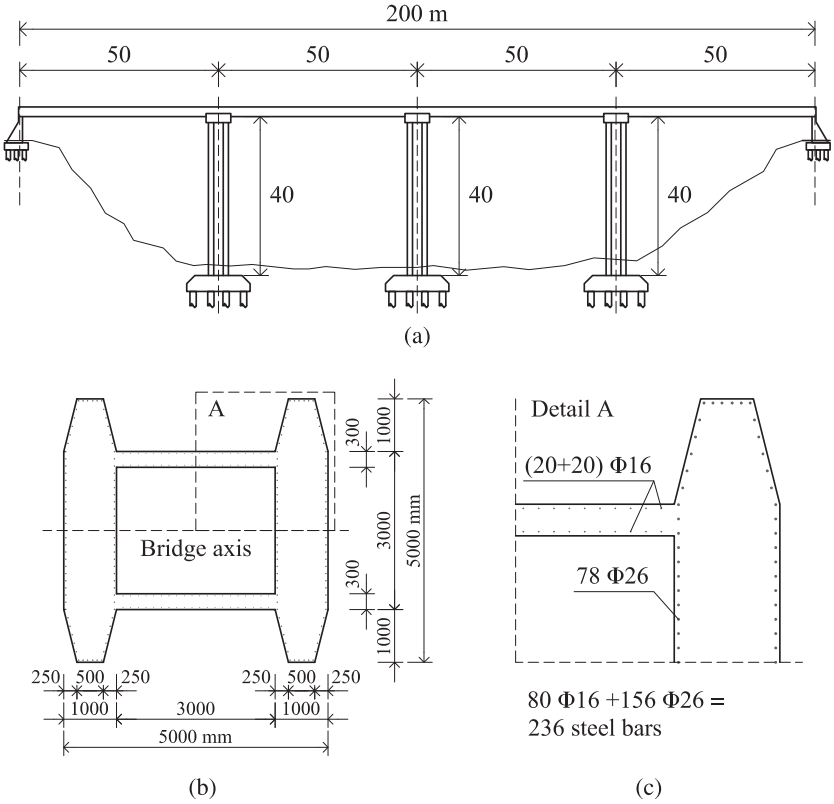

Figure 13. Continuous bridge. (a) Overall dimensions of the bridge. (b) Geometry, dimensions, and (c) detail of the reinforcement layout of the cross-section of the piers.

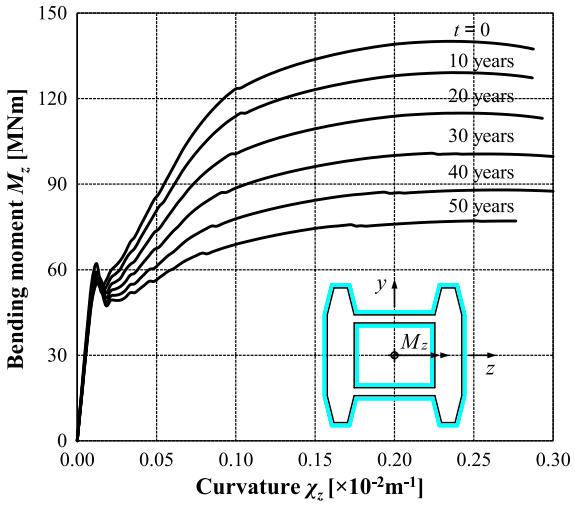

Figure 14. Bridge pier cross-section under corrosion. Nominal bending moment M_z versus curvature χ_z diagrams for $N = 25$MN over a 50-year lifetime with time steps $\Delta t = 10$ years.

provide only a measure of the dispersion of the results and do not indicate an increase over time of the system functionality and resilience.

In case of negligible idle time between the occurrence of the seismic event and the beginning of the recovery process ($t_i = t_0$) and time horizon limited to the final recovery time ($t_h = t_f$), the lifetime seismic resilience does not depend significantly on the recovery time interval δ_r [23]. The main factors in the assessment of seismic resilience include the loss of functionality ΔQ at time t_0, the functionality target Q_t to be reached at time t_f, and the recovery profile $r = r(t)$. The results of a parametric analysis aimed at investigating the role of these factors are presented in Figure 12 with reference to the mean values of seismic resilience.

It is noted that the expected loss of functionality due to seismic damage (Figure 12(a)) may significantly affect the lifetime seismic resilience. This highlights the importance of a proper modeling of both the lifetime deterioration process and the damage effects due to seismic events. The functionality target of the recovery process is also a key factor to improve the lifetime seismic resilience and to reduce the time effects of both deterioration and seismic damage (Figure 12(b)). Finally, the type of recovery profile is of prominent importance to ensure suitable levels of lifetime seismic resilience (Figure 12(c)). However, it is worth noting that the role of deterioration on lifetime resilience is not modified by the type of recovery process, because the ratio $R(t_0)/R(0)$ is almost independent on the recovery profile.

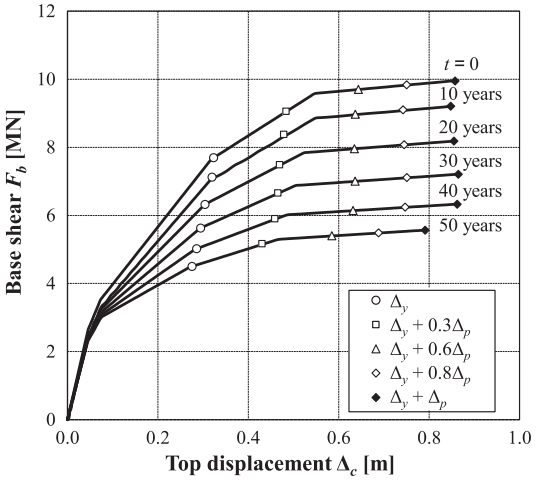

Figure 15. Bridge under corrosion. Nominal base shear F_b versus top displacement of the central pier Δ_c over a 50-year lifetime with time steps $\Delta t = 10$ years.

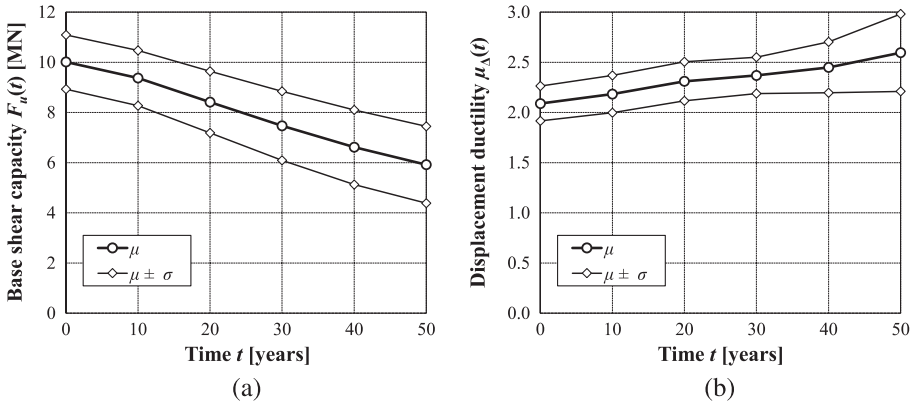

Figure 16. Bridge under corrosion. Time evolution of mean μ and standard deviation σ of (a) base shear capacity $F_u = F_u(t)$ and (b) displacement ductility $\mu_\Delta = \mu_\Delta(t)$.

5.3. Continuous concrete girder bridge

The seismic resilience of the four-span continuous concrete girder bridge shown in Figure 13(a) [28] is investigated. The total length of the bridge is 200 m, with spans of 50 m. The bridge deck is a two-box girder. The bridge piers have box cross-section with the geometry, nominal dimensions, and reinforcement layout shown in Figures 13(b) and 13(c). Connections of the deck to both piers and abutments are monolithic. The structure is considered fully fixed at the abutments and the base of the piers. The structure is analyzed by assuming a seismic weight $p = 300$ kN/m, including self-weight, dead loads, and a 20% of live loads, applied on the deck. The nominal values of the concrete and steel strength are $f_c = 30$ MPa and $f_{sy} = 500$ MPa, respectively. The strain limits are $\varepsilon_{cu} = 0.35\%$ for concrete in compression and $\varepsilon_{su} = 5.00\%$ for reinforcing steel of uncorroded bars.

The bridge piers are exposed to the diffusive attack of chlorides along the external and internal surface, because the hollow core is not hermetically closed over the height. The lifetime performance of the cross-section of the piers is shown in Figure 14 in terms of nominal bending moment M_z versus curvature χ_z diagrams under a compressive axial force $N = 25$ MN. The bending strength of the cross-section significantly decreases over lifetime. On the contrary, the ultimate curvature tends to slightly increase as the resisting cross-section of the steel bars in tension decreases due to corrosion. This initial trend is reversed after about 40 years because of the progressive deterioration of concrete in compression and the significant reduction of the reinforcing steel ductility.

At the system level, the deck is modeled by elastic beam elements, because under transversal loading the nonlinear behavior is expected to develop only in the piers. Elastic beam elements with

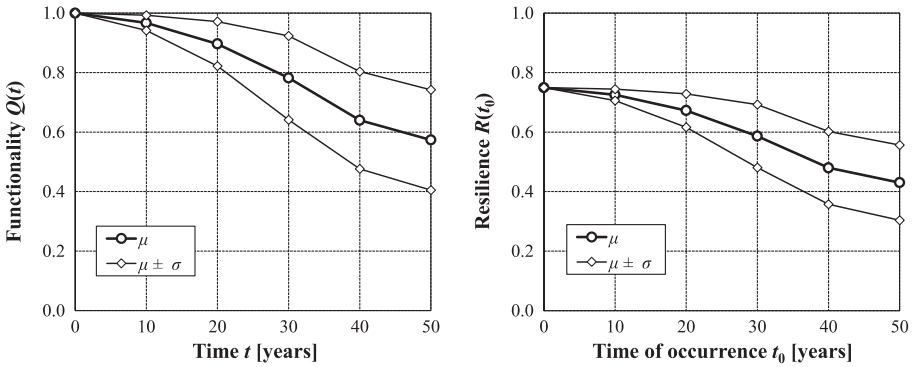

Figure 17. Bridge under corrosion. Time evolution of mean μ and standard deviation σ of (a) system functionality $Q = Q(t)$ and (b) seismic resilience $R = R(t_0)$ for the case of $t_i = t_0$, $t_h = t_f$, $\delta_r = 12$ months, functionality loss $\Delta Q(t_0) = 0.5Q(t_0)$, and recovery process with sinusoidal profile and partial restoring aimed at recovering the pre-event functionality.

Table V. Characteristics of the seismic records [66].

Earthquake record	Year	Station	Soil type [42]	Scaling factor	Scaled PGA [g]
EQ1 – Loma Prieta	1989	Hollister Diff. Array	D	2.0	0.54
EQ2 – Loma Prieta	1989	Gilroy Array #7	D	3.0	0.68
EQ3 – Landers	1992	Desert Hot Springs	C	4.1	0.62
EQ4 – Landers	1992	Yermo Fire Station	D	3.3	0.50
EQ5 – Cape Mendocino	1992	Rio Dell Overpass-FF	C	1.8	0.69
EQ6 – Superstition Hills	1987	Plaster City	D	3.3	0.61
EQ7 – Northridge	1994	Canoga Park-Topanga Can	D	1.8	0.64
EQ8 – Northridge	1994	Beverly Hills 14145 Mulhol	C	1.4	0.56
EQ9 – Northridge	1994	N Hollywood-Coldwater Can	C	2.6	0.69
EQ10 – Northridge	1994	Sunland-Mt. Gleason Ave	C	3.3	0.52

lumped inelastic rotational springs at member ends are used to model the piers. The bending moment-rotation constitutive laws are described by a stepwise linearization of the bending moment-curvature relationships integrated over the length of the plastic hinges. Further details on the moment-rotation constitutive laws can be found in [28].

Nonlinear static analyses of the bridge under uniform lateral forces applied at the deck level are carried out using the code Ruaumoko2D [63]. Figure 15 shows the lifetime performance of the bridge in terms of nominal total base shear F_b versus top displacement of the central pier Δ_c. The points corresponding to the displacement limits listed in Table I are also indicated on the capacity curves. These diagrams show a significant decrease over time of the base shear capacity $F_u = F_u(t)$.

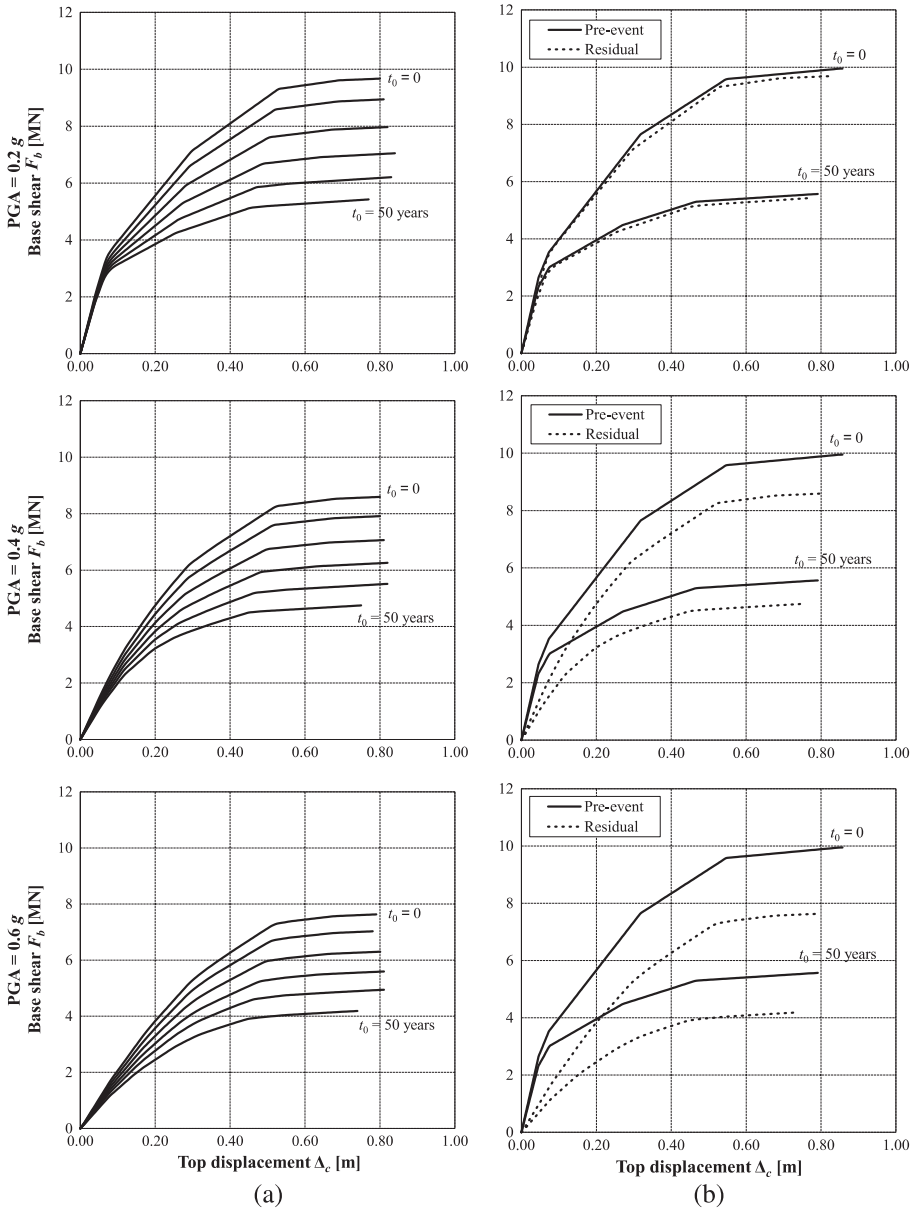

Figure 18. Bridge under corrosion. (a) Post-event mean capacity curves in terms of base shear F_b versus top displacement Δ_c of the nominal structure for the ensemble of earthquake records given in Table V with increasing level of peak ground acceleration PGA = 0.2 g, 0.4 g, and 0.6 g ($\Delta t_0 = 10$ years). (b) Comparison of pre-event (continuous line) and post-event (dashed lines) mean capacity curves F_b–Δ_c for $t_0 = 0$ and $t_0 = 50$ years.

On the contrary, an increase of displacement ductility $\mu_\Delta = \mu_\Delta(t)$ is observed mainly due to a reduction of the yielding displacement.

These results are confirmed also in probabilistic terms. Figure 16 shows the time evolution of the probabilistic parameters of the base shear capacity $F_u = F_u(t)$ and displacement ductility $\mu_\Delta = \mu_\Delta(t)$. The corresponding time evolution of the probabilistic parameters of the system functionality $Q = Q(t)$ associated with the performance functions $F_u = F_u(t)$ and $\mu_\Delta = \mu_\Delta(t)$ is shown in Figure 17(a). As expected, over time, the mean value of the functionality decreases and the effects of uncertainty tend to increase because of the deterioration process. This confirms that the seismic resilience $R = R(t_0)$ depends on the time t_0 of occurrence of the seismic event, as shown in Figure 17(b) for a case study with $t_i = t_0$, $t_h = t_f$, δ_r =12 months, functionality loss $\Delta Q(t_0) = 0.5Q(t_0)$, and recovery process with sinusoidal profile and partial restoring aimed at recovering the pre-event functionality.

The probabilistic analysis under a prescribed drop of system functionality ΔQ provides important information about the influence of deterioration on the time-variant seismic resilience. However, for deteriorating systems, the residual functionality $Q_r(t_0) = Q(t_0) - \Delta Q(t_0)$ after a seismic event depends also on the seismic performance available at time of occurrence t_0. To investigate the combined

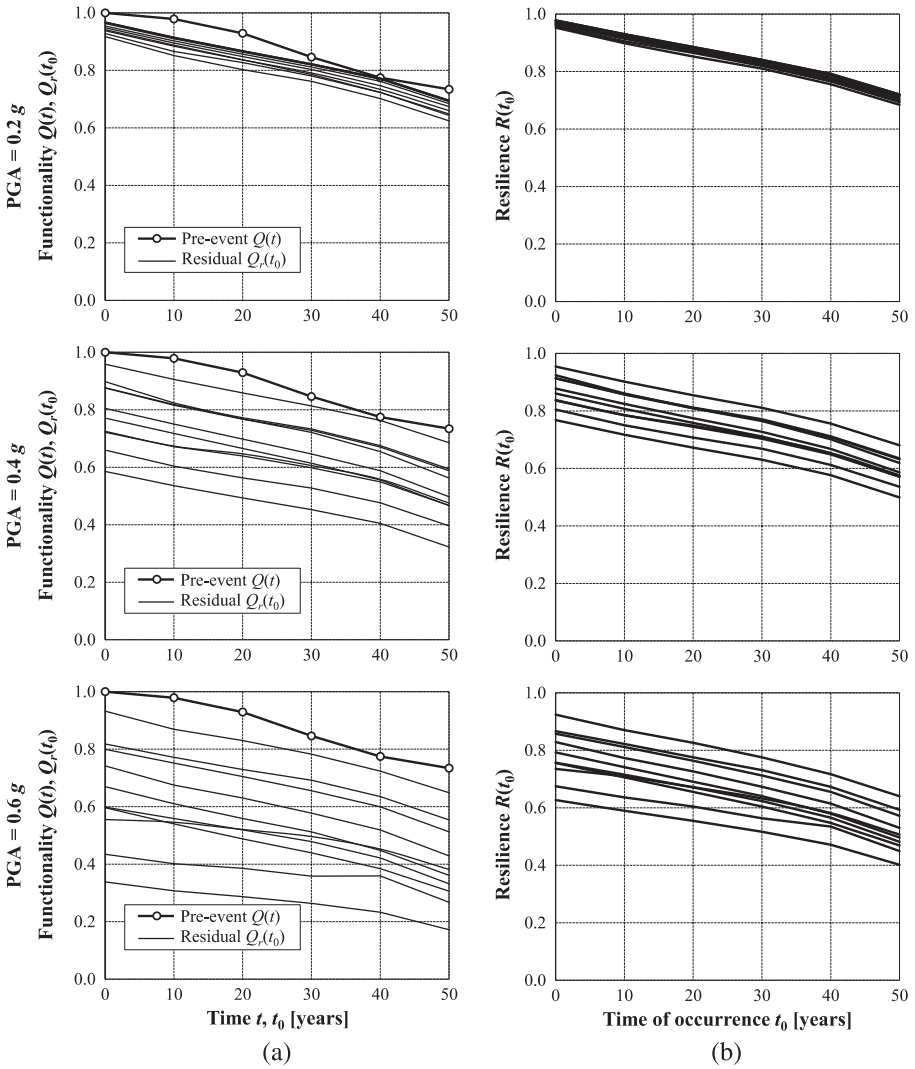

Figure 19. Bridge under corrosion. (a) Comparison of the nominal system functionality $Q = Q(t)$ of the corroded bridge to the nominal residual functionality curves $Q_r = Q_r(t_0)$ for the 10 earthquake records listed in Table V. (b) Nominal seismic resilience $R = R(t_0)$ associated with the 10 earthquake records for the case of $t_i = t_0$, $t_h = t_f$, δ_r =12 months, and recovery process with sinusoidal profile and partial restoring.

effects of seismic and environmental hazards, the residual functionality $Q_r = Q_r(t_0)$ of the bridge is evaluated by performing in sequence at time t_0 a nonlinear dynamic time-history analysis under ground motion, to assess the seismic damage, and a nonlinear static analysis, to achieve the post-event residual seismic capacity.

The nonlinear dynamic response of the bridge is investigated by using the code OpenSees [64]. The hysteretic rule of the rotational springs accounts for the seismic damage in terms of cyclic degradation of unloading stiffness, reloading stiffness, and strength [65]. Further details are given in [30]. The variability of the seismic action is considered with reference to the ensemble of ten earthquake records listed in Table V [66]. The mean response spectrum of these records matches reasonably well the Eurocode 8 response spectrum for soil class B and peak ground acceleration PGA $= 0.54\,g$ [42]. Nonlinear dynamic analyses of the nominal bridge structure are carried out every 10 years over a 50-year lifetime under the 10 earthquake records with increasing levels of seismic intensity PGA $= 0.2\,g$, $0.4\,g$, and $0.6\,g$. The post-event mean capacity curves in terms of base shear F_b versus top displacement Δ_c, obtained by nonlinear static analyses performed on the bridge structure in the configurations reached at the end of the seismic events, are shown in Figure 18(a). These curves include the combined effects of seismic damage and environmental deterioration. As expected, the effects of seismic damage depend on the time-variant deterioration process and increase as the seismic intensity increases. This is shown also in Figure 18(b), where the comparison of the pre- and post-event capacity curves for $t_0 = 0$ and $t_0 = 50$ years confirms that the drop of performance and functionality depends on the time of occurrence t_0.

Figure 19(a) compares the time evolution of the nominal system functionality $Q = Q(t)$ of the corroding bridge to the nominal residual functionality curves $Q_r = Q_r(t_0)$ associated with the 10 earthquake records listed in Table V. These results highlight the large variability of both the seismic damage and related drop of functionality with the characteristics of the earthquake records. However, the corresponding variability of seismic resilience $R = R(t_0)$ is reduced based on the effectiveness and rapidity of the recovery interventions, as shown in Figure 19(b) for $t_i = t_0$, $t_h = t_f$, $\delta_r = 12$ months, and recovery process with sinusoidal profile and partial restoring. Further research is necessary to generalize these results in probabilistic terms. However, they clearly indicate the importance of a multi-hazard life-cycle oriented approach to seismic design of resilient structure and infrastructure systems to limit the effects of aging and deterioration and to establish effective and rapid post-event recovery procedures.

6. CONCLUSIONS

A probabilistic approach to lifetime assessment of seismic resilience of concrete structures exposed to chloride-induced corrosion has been presented. The time-variant seismic performance has been evaluated at the system level based on a methodology for concrete structures in aggressive environment that accounts for both the diffusion process of chlorides and corrosion damage induced by diffusion. The corrosion modeling included the mass loss of steel bars, the reduction of steel ductility, and the deterioration of concrete strength because of the longitudinal splitting cracks and spalling of the concrete cover. The time-variant seismic capacity of the structural system under corrosion has been assumed as functionality indicator and seismic resilience has been evaluated with respect to this indicator over the structural lifetime. Based on the proposed approach, it has been shown that the effects of corrosion may reduce over time the system functionality and, consequently, make the seismic resilience depending on the time of occurrence of the seismic event. This dependence is emphasized by the uncertainty associated with the deterioration process, which leads to a remarkable increase over time of the random variability of both functionality and resilience.

The results of a parametric analysis performed for a three-story frame building under corrosion of the columns showed that the impact of continuous deterioration on the seismic performance and functionality under uncertainty may be dramatic, particularly when the reduction of base shear capacity is associated with a change in the location of the flexural plastic hinges with the possible activation of collapse mechanisms with limited ductility and energy dissipation capacity. Moreover, it has been found that the main factors affecting the lifetime seismic resilience under continuous

deterioration include the drop of functionality induced by the seismic event, the functionality target of the recovery interventions, and the recovery profile. In particular, the drop of functionality is also time-dependent because of the combined effects of structural deterioration and seismic damage. These effects have been taken into account based on a sequence of nonlinear dynamic analysis under ground motion and post-event nonlinear static analysis of the deteriorating structure. This procedure has been applied by considering the effects of single mainshocks, but it is worth noting that it could be used to account also for the cumulative seismic damage induced by multiple mainshocks or mainshock-aftershock sequences. The results obtained for a continuous girder bridge under corrosion of the piers showed a significant variability of both the seismic damage and related drop of functionality depending on the characteristics of the earthquake records. However, the corresponding variability of the seismic resilience is mitigated by the effects of the recovery interventions. These results highlighted the importance of a multi-hazard life-cycle oriented approach to seismic design of resilient structure and infrastructure systems to limit the effects of aging and deterioration and to establish effective and rapid post-event recovery procedures.

Further research is required to formulate and validate nonlinear or constant stepwise probabilistic functionality indicators based on seismic capacity thresholds and/or discrete functionality states. This paper focused on the seismic resilience of single structures, but the proposed approach could be extended to infrastructure systems, such as bridge networks, by means of suitable system functionality indicators able to account for the functionality losses consequent to the effects of continuous deterioration and sudden seismic damage suffered by the system components. Moreover, the role of several factors of the recovery process should be further investigated in probabilistic terms, including idle time, recovery time, target functionality, time horizon, and recovery profiles with time-variant parameters related to type, magnitude, and location of seismic damage. Finally, the effects of maintenance activities and repair interventions need to be incorporated in the proposed framework for the lifetime probabilistic assessment of seismic resilience of deteriorating concrete structures.

REFERENCES

1. Ellingwood BR. Risk-informed condition assessment of civil infrastructure: state of practice and research issues. *Structure and Infrastructure Engineering* 2005; **1**(1):7–18. DOI:10.1080/15732470412331289341.
2. Frangopol DM. Life-cycle performance, management, and optimization of structural systems under uncertainty: accomplishments and challenges. *Structure and Infrastructure Engineering* 2011; **7**(6):389–413. DOI:10.1080/15732471003594427.
3. FEMA. *Planning for a Sustainable Future: The Link Between Hazard Mitigation and Livability*. Federal Emergency Management Agency: Washington, DC, USA, 2000.
4. Wachtendorf T, Connell R, Tierney KJ, Kompanik K. *Disaster Resistant Communities Initiative: Assessment of the Pilot Phase – Year 3*. Disaster Research Center, University of Delaware: Newark, DE, USA, 2002.
5. JCSS. Risk assessment in engineering. Principles, system representation & risk criteria. Joint Committee on Structural Safety, Technical University of Denmark, Lingby, Denmark, 2008.
6. Erath A, Birdsall J, Axhausen KW, Hajdin R. Vulnerability assessment methodology for Swiss road network. *Journal of the Transportation Research Board* 2009; No. 2137: 118–126, Transportation Research Board of the National Academies, TRB, Washington, DC, USA. DOI: 10.3141/2137-13.
7. Holling CS. Resilience and stability of ecological systems. *Annual Review of Ecology and Systematics* 1973; **4**:1–23. DOI:10.1146/annurev.es.04.110173.000245.
8. McAslan A. *The Concept of Resilience. Understanding its Origins, Meaning and Utility*. Torrens Resilience Institute: Adelaide, Australia, 2010.
9. Gilbert SW. Disaster resilience: a guide to the literature. NIST Special Publication 1117, National Institute of Standards and Technology, Office of Applied Economics Building and Fire Research Laboratory, Gaithersburg, MD, USA, 2010.
10. Bruneau M, Chang SE, Eguchi RT, Lee GC, O'Rourke TD, Reinhorn AM, Shinozuka M, Tierney KJ, Wallace WA, von Winterfeldt D. A framework to quantitatively assess and enhance the seismic resilience of communities. *Earthquake Spectra* 2003; **19**(4):733–752. DOI:10.1193/1.1623497.
11. Rose A. Defining and measuring economic resilience to disasters. *Disaster Prevention and Management* 2004; **13**(4):307–314. DOI:10.1108/09653560410556528.
12. Chang SE, Pasion C, Tatebe K, Ahmad R. Linking lifeline infrastructure performance and community disaster resilience: models and multi-stakeholder processes. Technical Report MCEER-08-0004. Multidisciplinary Center for Earthquake Engineering Research, State University of New York at Buffalo, Buffalo, NY, USA, 2008.
13. Renschler CS, Frazier AE, Arendt LA, Cimellaro GP, Reinhorn AM, Bruneau M. A framework for defining and measuring resilience at the community scale: the PEOPLES resilience framework. Technical Report MCEER-10-0006. Multidisciplinary Center for Earthquake Engineering Research, State University of New York at Buffalo, Buffalo, NY, USA, 2010.

14. Cimellaro GP, Reinhorn AM, Bruneau M. Framework for analytical quantification of disaster resilience. *Engineering Structures* 2010; **32**(11):3639–3649. DOI:10.1016/j.engstruct.2010.08.008.
15. Fischinger M (ed.). *Performance-Based Seismic Engineering: Vision for an Earthquake Resilient Society*. Geotechnical, Geological and Earthquake Engineering Book Series. Springer: Dordrecht, The Netherlands, 2014. DOI: 10.1007/978-94-017-8875-5.
16. Bocchini P, Decò A, Frangopol DM. Probabilistic functionality recovery model for resilience analysis. *Sixth International Conference on Bridge Maintenance*, *Safety and Management* (IABMAS 2012), Stresa, Italy, July 8–12, 2012. In: *Bridge Maintenance*, *Safety*, *Management*, *Resilience and Sustainability*, Biondini F, Frangopol DM (Eds.), CRC Press/Balkema, Taylor & Francis Group, London, UK, 2012.
17. Decò A, Bocchini P, Frangopol DM. A probabilistic approach for the prediction of seismic resilience of bridges. *Earthquake Engineering and Structural Dynamics* 2013; **42**(10):1469–1487. DOI:10.1002/eqe.2282.
18. Chang SE, Shinozuka M. Measuring improvements in the disaster resilience of communities. *Earthquake Spectra* 2004; **20**(3):739–755. DOI:10.1193/1.1775796.
19. Bruneau M, Reinhorn AM. Exploring the concept of seismic resilience for acute care facilities. *Earthquake Spectra* 2007; **23**(1):41–62. DOI:10.1193/1.2431396.
20. Cimellaro GP, Christovasilis IP, Reinhorn AM, De Stefano A, Kirova T. L'Aquila earthquake of April 6, 2009 in Italy: rebuilding a resilient city to multiple hazard. Technical Report MCEER-10-0010. Multidisciplinary Center for Earthquake Engineering Research, State University of New York at Buffalo, Buffalo, NY, USA, 2010.
21. Cimellaro GP, Reinhorn AM, Bruneau M. Seismic resilience of a hospital system. *Structure and Infrastructure Engineering* 2010; **6**(1–2):127–144. DOI:10.1080/15732470802663847.
22. Bocchini P, Frangopol DM. Restoration of bridge networks after an earthquake: multi-criteria intervention optimization. *Earthquake Spectra* 2012; **28**(2):426–455. DOI:10.1193/1.4000019.
23. Titi A, Biondini F. Resilience of concrete frame structures under corrosion. *11th International Conference on Structural*, *Safety* & *Reliability* (ICOSSAR 2013), New York, NY, USA, June 16–20, 2013. In: *Safety*, *Reliability*, *Risk and Life-Cycle Performance of Structures and Infrastructures*, Deodatis D, Ellingwood BR, Frangopol DM (Eds.), CRC Press/Balkema, Taylor & Francis Group, London, UK, 2014.
24. Biondini F, Bontempi F, Frangopol DM, Malerba PG. Cellular automata approach to durability analysis of concrete structures in aggressive environments. *Journal of Structural Engineering* 2004; **130**(11):1724–1737. DOI:10.1061/(ASCE)0733-9445(2004)130:11(1724).
25. Biondini F, Bontempi F, Frangopol DM, Malerba PG. Probabilistic service life assessment and maintenance planning of concrete structures. *Journal of Structural Engineering* 2006; **132**(5):810–825. DOI:10.1061/(ASCE)0733-9445(2006)132:5(810).
26. Biondini F, Frangopol DM. Probabilistic limit analysis and lifetime prediction of concrete structures. *Structure and Infrastructure Engineering* 2008; **4**(5):399–412. DOI:10.1080/15732470701270157.
27. Biondini F, Palermo A, Toniolo G. Seismic performance of concrete structures exposed to corrosion: case studies of low-rise precast buildings. *Structure and Infrastructure Engineering* 2011; **7**(1–2):109–119. DOI:10.1080/15732471003588437.
28. Biondini F, Camnasio E, Palermo A. Lifetime seismic performance of concrete bridges exposed to corrosion. *Structure and Infrastructure Engineering* 2014; **10**(7):880–900. DOI:10.1080/15732479.2012.761248.
29. UN/ISDR. Global assessment report on disaster risk reduction. *United Nations International Strategy for Disaster Reduction*, *Geneva*, *Switzerland*, 2009.
30. Camnasio E. Lifetime performance and seismic resilience of concrete structures exposed to corrosion. PhD Thesis, Politecnico di Milano, Milan, Italy, 2013.
31. Kim S, Frangopol DM, Soliman M. Generalized probabilistic framework for optimum inspection and maintenance planning. *Journal of Structural Engineering* 2013; **139**(3):435–447. DOI:10.1061/(ASCE)ST.1943-541X.0000676.
32. Barone G, Frangopol DM, Soliman M. Optimization of life-cycle maintenance of deteriorating structures considering expected annual system failure rate and expected cumulative cost. *Journal of Structural Engineering* 2014; **140**(2):1–13. DOI:10.1061/(ASCE)ST.1943-541X.0000812.
33. ASCE. Report card for America's infrastructure. American Society of Civil Engineers, 2013.
34. Bocchini P, Frangopol DM. Optimal resilience- and cost-based postdisaster intervention prioritization for bridges along a highway segment. *Journal of Bridge Engineering* 2012; **17**(1):117–129. DOI:10.1061/(ASCE)BE.1943-5592.0000201.
35. Çağnan Z, Davidson RA, Guikema SD. Post-earthquake restoration planning for Los Angeles electric power. *Earthquake Spectra* 2006; **22**(3):589–608. DOI:10.1193/1.2222400.
36. Cimellaro GP, Reinhorn AM, Bruneau M. Quantification of seismic resilience. *8th U.S. National Conference of Earthquake Engineering*, San Francisco, CA, USA, April 18–22, 2006, Earthquake Engineering Research Institute, EERI.
37. Rose A, Benavides J, Chang SE, Szczesniak P, Lim D. The regional economic impact of an earthquake: direct and indirect effects of electricity lifeline disruptions. *Journal of Regional Science* 1997; **37**(3):437–458. DOI:10.1111/0022-4146.00063.
38. Shinozuka M. Resilience and sustainability of infrastructure systems. In: *Frontier Technologies for Infrastructures Engineering*, Chen SS, Ang AHS (eds.). Structures and Infrastructures Book Series. CRC Press/Balkema, Taylor & Francis Group: London, UK, 2009.
39. Xu N, Guikema SD, Davidson RA, Nozick LK, Çağnan Z, Vaziri K. Optimizing scheduling of post-earthquake electric power restoration tasks. *Earthquake Engineering and Structural Dynamics* 2007; **36**(2):265–284. DOI:10.1002/eqe.623.

40. FEMA. HAZUS-MH MR4 earthquake model user manual. Department of Homeland Security, Federal Emergency Management Agency, Washington, DC, USA, 2009.
41. Mander JB, Dhakal RP, Mashiko N, Solberg KM. Incremental dynamic analysis applied to seismic financial risk assessment of bridges. *Engineering Structures* 2007; **29**(10):2662–2672. DOI:10.1016/j.engstruct.2006.12.015.
42. CEN-EN 1998–1. Eurocode 8: Design of structures for earthquake resistance. Part 1: general rules, seismic actions and rules for buildings. European Committee for Standardization, Brussels, Belgium, 2004.
43. Biondini F, Toniolo G, Tsionis G. Capacity design and seismic performance of multi-storey precast structures. *European Journal of Environmental and Civil Engineering* 2010; **14**(1):11–28. DOI:10.1080/19648189.2010.9693198.
44. Paulay T, Priestley MJN. *Seismic Design of Reinforced Concrete and Masonry Buildings*. John Wiley & Sons: New York, NY, USA, 1992.
45. Kafali C, Grigoriu M. Rehabilitation decision analysis, *9th International Conference on Structural Safety and Reliability* (ICOSSAR'05), Rome, Italy, June 19–23, 2005. In: *Safety and Reliability of Engineering Systems and Structures*, Augusti G, Schuëller G, Ciampoli M (eds.). Millpress: Rotterdam, The Netherlands, 2005.
46. Akiyama M, Frangopol DM, Matsuzaki H. Life-cycle reliability of RC bridge piers under seismic and airborne chloride hazards. *Earthquake Engineering and Structural Dynamics* 2011; **40**(15):1671–1687. DOI:10.1002/eqe.1108.
47. Titi A, Biondini F. Probabilistic seismic assessment of multistory precast concrete frames exposed to corrosion. *Bulletin of Earthquake Engineering* 2014; **12**(6):2665–2681. DOI:10.1007/s10518-014-9620-2.
48. Chiu CK, Tu FJ, Hsiao FP. Lifetime seismic performance assessment for chloride-corroded reinforced concrete buildings. *Structure and Infrastructure Engineering* 2015; **11**(3):345–362. DOI:10.1080/15732479.2014.886596.
49. Bertolini L, Elsener B, Pedeferri P, Polder R. *Corrosion of Steel in Concrete. Prevention, Diagnosis and Repair*. Wiley-VCH: Weinheim, Germany, 2004.
50. Glicksman ME. *Diffusion in Solids*. John Wiley & Sons: New York, NY, USA, 2000.
51. Titi A, Biondini F. On the accuracy of diffusion models for life-cycle assessment of concrete structures. *Structure and Infrastructure Engineering* (submitted).
52. fib. Model Code for service life design. Bulletin 34, Fédération internationale du béton / International Federation for Structural Concrete, 2006.
53. Almusallam AA. Effect of degree of corrosion on the properties of reinforcing steel bars. *Construction and Building Materials* 2001; **15**(8): 361–368. DOI: 10.1016/S0950-0618(01)00009-5.
54. Apostolopoulos CA, Papadakis VG. Consequences of steel corrosion on the ductility properties of reinforcement bar. *Construction and Building Materials* 2008; **22**(12):2316–2324. DOI:10.1016/j.conbuildmat.2007.10.006.
55. Cabrera JG. Deterioration of concrete due to reinforcement steel corrosion. *Cement & Concrete Composites* 1996; **18**(1):47–59. DOI:10.1016/0958-9465(95)00043-7.
56. Vidal T, Castel A, François R. Analyzing crack width to predict corrosion in reinforced concrete. *Cement and Concrete Research* 2004; **34**(1):165–174. DOI:10.1016/S0008-8846(03)00246-1.
57. Al-Harthy AS, Stewart MG, Mullard J. Concrete cover cracking caused by steel reinforcement corrosion. *Magazine of Concrete Research* 2011; **63**(9):655–667. DOI:10.1680/macr.2011.63.9.655.
58. Biondini F, Vergani M. Deteriorating beam finite element for nonlinear analysis of concrete structures under corrosion. *Structure and Infrastructure Engineering* 2015; **11**(4):519–532. DOI:10.1080/15732479.2014.951863.
59. Pastore T, Pedeferri P. La corrosione e la protezione delle opere metalliche esposte all'atmosfera (In Italian). *L'edilizia* 1994; December: 75–92.
60. Liu T, Weyers RW. Modeling the dynamic corrosion process in chloride contaminated structures. *Cement and Concrete Research* 1998; **28**(3):365–379. DOI:10.1016/S0008-8846(98)00259-2.
61. Thoft-Christensen P. Assessment of the reliability profiles for concrete bridges. *Engineering Structures* 1998; **20**(11):1004–1009. DOI:10.1016/S0141-0296(97)00196-X.
62. CEB. Model Code for seismic design of concrete structures. Bulletin 165, Comité européen du béton, 1985.
63. Carr AJ. RUAUMOKO program for inelastic dynamic analysis. Department of Civil Engineering, University of Canterbury: Christchurch, New Zealand, 2008.
64. Mazzoni S, McKenna F, Scott MH, Fenves GL, *et al*. Open System for Earthquake Engineering Simulation (OpenSees). OpenSees Command Language Manual. Pacific Earthquake Engineering Research Center (PEER), College of Engineering, University of California, Berkeley, CA, USA, 2006.
65. Lowes LN, Mitra N, Altoontash A. A beam-column joint model for simulating the earthquake response of reinforced concrete frames. Pacific Earthquake Engineering Research Center, College of Engineering, University of California: Berkeley, CA, USA, 2003.
66. Pampanin S, Christopoulos C, Priestley MJN. *Residual deformations in the performance-based seismic assessment of frame structures*. IUSS Press: Pavia, Italy, 2002.